Macromolecules

ARTICLE

pubs.acs.org/Macromolecules

Structure and Mechanical Behavior of Elastomeric Multiblock Terpolymers Containing Glassy, Rubbery, and Semicrystalline Blocks

Feng Zuo, C. Guillermo Alfonzo,† and Frank S. Bates*

Department of Chemical Engineering and Materials Science, University of Minnesota, Minneapolis, Minnesota 55455, United States

Supporting Information

ABSTRACT: Multiblock copolymers containing glassy poly(cyclohexylethylene) (C), rubbery poly(ethylene-*alt*-propylene) (P), and semicrystalline poly(ethylene) (E) were synthesized by sequential anionic polymerization of styrene, isoprene, and butadiene followed by catalytic hydrogenation. The resulting CECP-CEC (denoted XPX) and CECP (XP) multiblock copolymers each contain 50 vol % of P and equal amounts of C and E. These materials have been studied by dynamic mechanical spectroscopy (DMS), transmission electron microscopy (TEM), small- and wide-angle X-ray scattering (SAXS and WAXS), differential scanning calorimetry (DSC), and tensile deformation to characterize the morphology, phase behavior, and mechanical properties. Microphase separation in these compounds is induced by crystallization of E and/or chemical incompatibility between the three blocks, leading to a new type of morphology which contains continuous region of P and continuous region of microphase-separated X, resulting in mechanically resilient materials. High molecular weight block copolymers microphase separate with two different length scales associated with segregation between C and E and X and P. These structural features produce a nonclassical scaling relationship for the C−E domain spacing, $d \sim N^{0.31}$, where N is the degree of polymerization of CEC portion. The role of semicrystalline E domains during uniaxial deformation has been exposed with WAXS experiments, which support a two-step mechanism involving recoverable and nonrecoverable deformation to different extents. Strain hardening is observed in double-anchored XPX, but not in single-anchored XP, at large tensile strains.

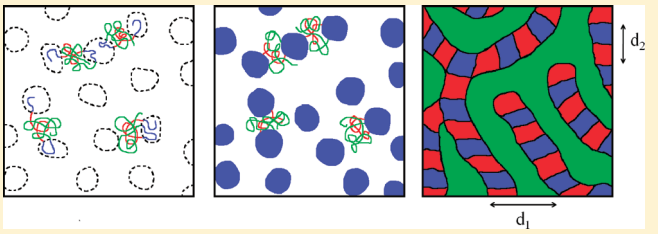

INTRODUCTION

Most applications of block copolymers rely on a state of microphase separation, which combines the physical and chemical properties of two or more materials in a single macromolecular compound. Different microdomain geometries offer a portfolio of distinctly different properties. For instance, rubbery spheres in a glassy matrix can improve impact resistance, while glassy spheres in rubbery matrix may enhance mechanical strength.[1,2] For two-monomer systems, including AB diblock and ABA triblock, self-consistent field theory (SCFT) has established quantitative relationships between composition, overall molecular weight, the segment−segment interaction parameter χ_{AB}, and the microdomain geometry.[3−6] (Notwithstanding the general completeness and predictive nature of this theory, recent experiments have revealed additional, unanticipated phases.[7]) Addition of a third block type (e.g., ABC triblock) greatly expands the portfolio of ordered phases and complicates the theory.[8] Today there are more than 30 documented ABC ordered morphologies, and this list is likely to grow much larger. While the introduction of additional blocks adds structural complexity, it also provides the potential for enhanced control over a host of physical properties. This article describes the structure and properties of multiblock terpolymers that combine glassy, rubbery, and semicrystalline blocks into specific molecular architectures that result in mechanically robust and resilient materials.

Block copolymers containing glassy, rubbery, and semicrystalline blocks have not received much attention.[9−19] Balsamo et al.[9−11] prepared ABC triblock copolymers of poly(styrene), poly(butadiene), and poly(ε-caprolactone), in which A is glassy, B is rubbery, and C is semicrystalline, and reported a core−shell cylinder morphology in a glassy matrix and high elongations at break attributed to confinement of semicrystalline poly(ε-caprolactone) within the cylinders. Schmalz et al.[12,13] studied block copolymers with the same architecture using poly(styrene), poly(ethylene-*alt*-propylene), and poly(ethylene) blocks. The dispersed glassy cylinders and poly(ethylene) crystals, embedded in a rubbery matrix, lead to a higher elastic modulus in deformation and less elastic recovery upon relaxation than conventional rubbers.

During the past decade our research group has investigated various multiblock systems ranging from conventional linear ABA triblocks to ABABA, ABCBA, and other pentablocks, a ABACABA heptablock architecture, and more.[16−25] A central theme of this program is to develop enhanced mechanical properties, particularly strength and toughness, based on judicious combinations of the basic mechanical properties offered by glassy, rubbery, and semicrystalline polymers. Saturated hydrocarbon polymers obtained through the heterogeneous catalytic saturation of poly(styrene) and poly(dienes) provide a powerful and commercially viable pallet of building blocks. Hydrogenation

Received: July 19, 2011
Revised: August 25, 2011
Published: September 28, 2011

of poly(styrene) yields glassy poly(cyclohexylethylene) (C) ($T_g \cong 147$ °C), while saturation of poly(1,4-butadiene) leads to semicrystalline poly(ethylene) (E) ($T_m \cong 110$ °C for the resulting linear low-density material). Rubbery blocks can be prepared by hydrogenating poly(1,4-isoprene) or poly(1,2-butadiene), resulting in poly(ethylene-*alt*-propylene) (P) ($T_g \cong -60$ °C) and poly(ethylethylene) (E_e) ($T_g \cong -20$ °C), respectively. C, E, and P can be prepared with any block sequence due to similar reactivity of the parent monomers during anionic polymerization. Moreover, coupling chemistry affords the opportunity to efficiently generate palindrome sequences, e.g., ABCBA or ABACABA.

Earlier work with various triblock, tetrablock, and pentablock copolymers formed from C and E demonstrated the importance of bridging versus dangling blocks in establishing mechanical toughness.[20−23] Terminal semicrystalline E blocks were most detrimental while adding bridging blocks of either E or C greatly enhanced the strain at break in tensile experiments. Complementary work performed with $(EP)_n$ multiblocks demonstrated the synergistic effects of crystallinity on elastic strength and the role that crystallization plays in inducing microphase separation between nearly compatible E and P blocks.[24,25] These studies also resulted in quantitative relationships for the temperature dependent interaction parameters (χ_{ij}) between C, E, and P, which are instrumental in guiding the design of multiblock terpolymers.

Mahanthappa et al.[16] produced a series of block copolymers, including CPC, CPEPC, and CEC, gradually substituting semicrystalline E blocks for the rubbery P block in a traditional glassy−rubbery thermoplastic elastomer (TPE) and documented an increase of elastic modulus and yield stress but a decrease of ultimate stress and fracture strain as the E fraction was increased. More recently, Bishop et al.[14] reported another type of saturated hydrocarbon TPE with an ABCBA molecular architecture. Short semicrystalline end blocks (A) are separated from long rubbery center blocks (C) by glassy B blocks. Crystallization from the homogeneous melt leads to formation of a layer rich in glassy block which surrounds the crystals.

Fleury et al.[18] designed a series of linear CECEC-P multiblock copolymers consisting of a compositionally symmetric CECEC sequence attached to a rubbery P block. A perpendicular lamellae in parallel lamellae morphology was found in shear-aligned high molecular weight samples. This interesting morphology was attributed to the sequence of interaction parameters $\chi_{EP} \ll \chi_{CP} < \chi_{CE}$, which most favors contacts between E and P and least favors those between C and E in conflict with the block sequence. This report details one of the few experimental observations of hierarchical structure with different domain sizes in bulk block copolymers,[26−33] which has motivated new theoretical work.[34−36] In contrast, low molecular weight CECEC-P and $(CECEC)_2$-P materials were melt disordered and appeared to show a crystallization-induced bicontinuous morphology at room temperature as indicated by TEM. The mechanical properties of these materials reportedly depend on the mode of segregation (induced by crystallization versus chemical incompatibility) and the chain architecture. Samples with a singly tethered P block (CECEC-P) support lower stresses and have a higher residual strain due to the slippage between P blocks, while $(CECEC)_2$-P exhibits greater recoverability and a higher ultimate stress due to the double-ended anchoring.[37,38]

In a previous work,[19] elastomeric multiblock copolymers in the form of CEC-P-CEC (or XPX) were synthesized and studied in terms of phase behavior and mechanical properties. This particular molecular design avoids melt ordering over a wide range of molecular weights ($M_n \lesssim 10^2$ kg/mol), which brings advantages for industrial processing, because ideally the processing temperature should be higher than the order−disorder transition temperature (T_{ODT}). Upon cooling, the homogeneous XPX materials microphase separate due to crystallization of the E blocks, yielding strong TPEs. Other materials with crystallization induced microphase segregation have been reported, but to the best of our knowledge, none show the combination of strength and recoverability of XPX.[39−41] The current study reports the synthesis and structural properties of higher molecular weight XPX materials and a XP tetrablock copolymer, with $f_C \approx f_E \approx 0.25$ and $f_P \approx 0.5$. These melt ordered multiblock copolymers are compared to the homologous melt disordered specimens considered previously, providing a comprehensive understanding of the relationships that govern microphase separation and mechanical behavior in these hierarchical compounds.

EXPERIMENTAL SECTION

Block Copolymer Synthesis and Molecular Characterization. Multiblock copolymers with chain architecture CECPCEC or CECP were synthesized by sequential anionic polymerization and catalytic hydrogenation. A detailed procedure was described in a previous publication.[19] Number-average molecular weights (M_n) of the first poly(styrene) blocks and molecular weight distributions (M_w/M_n) of multiblock products were analyzed by size exclusion chromatography (SEC). Volume fractions of S, B, and I were calculated according to ^{1}H nuclear magnetic resonance (NMR) spectra and published homopolymer densities at 140 °C ($\rho_S = 0.969$, $\rho_B = 0.826$, $\rho_I = 0.830$ g/cm^3)[42] and were converted to volume fractions of C, E, and P in the saturated materials. From these fractions and the M_n of the first poly(styrene) block, we can determine the overall M_n of CECPCEC and CECP. On the basis of the pseudo di- or triblock geometry, we will refer to CECPCEC as XPX, and CECP as XP, where X represents the CEC part of the copolymer.

Differential Scanning Calorimetry (DSC). DSC was carried out using TA Instruments Q1000 with a heating or cooling rate of 10 °C/min. The reported melting and crystallization temperatures were based on the peak position of endo- and exotherms. The crystallinity of poly(ethylene) was calculated using the expression $X_c = \Delta H_m/H^\circ_{m,E} \times w_E$, where $H^\circ_{m,E} = 277$ J/g^{-1} is the theoretical heat of melting for the 100% crystalline poly(ethylene),[43] w_E is the weight fraction of E block, and ΔH_m is the area under the melting peak.

Dynamic Mechanical Spectroscopy (DMS). Dynamic storage (G') and loss (G'') moduli were measured using a Rheometrics Scientific ARES rheometer in two types of tests: isothermal frequency sweep and isochronal temperature ramp. For the former test, measurements were conducted over the frequency range $0.01 \leq \omega \leq 100$ rad/s at selected temperatures, while in the latter one, the frequency was fixed and the temperature was varied at a constant rate. All measurements were conducted at a strain of 1 or 2%, within the linear viscoelastic regime.

Small-Angle X-ray Scattering (SAXS). Synchrotron SAXS was performed at the DuPont−Northwestern−Dow Collaborative Access Team (DND-CAT) beamline at the Advanced Photon Source with a X-ray wavelength of 0.729 Å and a sample-to-detector distance of 6.11 m. 2D SAXS patterns were acquired after holding specimens for 5 min at a target temperature. All X-ray scattering images were corrected for background scattering, and the intensities were normalized using a beam monitor. 2-dimensional data were reduced to the 1-dimensional form of intensity versus the magnitude of the scattering wave vector, $q = 4\pi\lambda^{-1}\sin(\theta/2)$, by azimuthal averaging.

Wide-Angle X-ray Scattering (WAXS). WAXS experiments were conducted at the Characterization Facility at the University of

Table 1. Molecular Characterization Data of XPX-2 and XP-2 Materials

sample	f_C[a]	f_E[a]	f_P[a]	M_n[b] (kg/mol)	M_w/M_n	T_{ODT} (°C)[c]	T_m(E) (°C)[d]	T_c(E) (°C)[d]	X_c(E) (%)[e]	T_g(P) (°C)[f]	T_g(C) (°C)[g]
XPX-2a	0.25	0.26	0.49	59	1.11	$<T_m$	98	54	22	−57	
XPX-2b	0.25	0.26	0.49	79	1.13	$<T_m$	95	53	16	−58	
XPX-2c	0.25	0.26	0.49	114	1.16	160−220	93	55	19	−57	
XPX-2d	0.27	0.25	0.48	133	1.13	220−260	87	55	19	−59	128
XPX-2e	0.26	0.25	0.49	195	1.14	270−310	88	57	18	−59	135
XP-2	0.25	0.25	0.50	86	1.08	200−240	94	58	15	−58	133

[a] Volume fraction based on ^{1}H NMR of the unsaturated precursors. [b] Determined by SEC from unsaturated multiblock precursors. [c] Order−disorder transition temperature probed by DMS and SAXS. [d] Peak melting or crystallinity temperature. [e] Crystallinity in E block. [f] Glass transition temperature for P block determined by DSC. [g] Glass transition temperature for C block determined by DMS.

Minnesota. 2D WAXS patterns were collected in transmission mode using a Bruker AXS Microdiffractometer with Cu Kα X-rays and a sample-to-detector distance of 59 mm. Polymer specimens were uniaxially deformed using a tensile tester, fixed at a specified strain using a homemade sample holder, and then mounted on the Microdiffractometer sample stage. The time delay between the ex-situ stretching and WAXS measurement is usually about 3 min.

Transmission Electron Microscopy (TEM). TEM experiments were also conducted at the Characterization Facility at the University of Minnesota with a FEI Tecnai T12 electron microscope. Samples were first trimmed to produce a flat surface and subsequently stained by exposure to ruthenium tetroxide (RuO_4) vapor from solution for about 4 h using reported procedures.[44] Stained samples were again cryomicrotomed at −120 °C, and about 60−90 nm thick sections were collected for TEM imaging.

Tensile Testing. Samples were uniaxially deformed in a Rheometrics Scientific Minimat tensile tester. All experiments were conducted at a constant rate of 100% strain per minute. Rectangular tensile bars about 11 mm long, 3 mm wide, and 1.2 mm thick were employed. The results reported in this study represent averages over at least five specimens tested per material. Loading and unloading cycles, i.e. step-cyclic tests, were employed with progressively increasing strains. Each strain step was followed by an unloading step, which returned the sample length to its original value; this may result in a small degree of buckling due to permanent set. A series of steps with increments of 50% were employed with XPX, while for XP only four strain cycles (100%, 200%, 400%, and 600%) were imposed sequentially. Strain cycles were applied continuously without any time delays.

RESULTS AND ANALYSIS

Synthesis. Multiblock copolymers XPX-2d, XPX-2e, and XP-2 were successfully synthesized. SEC traces show relatively monomodal and narrow molecular weight distributions, and ^{1}H NMR spectra confirm the complete hydrogenation of unsaturated precursors (see Supporting Information). These multiblock copolymers contain approximately 50 vol % P and 50 vol % CEC divided equally between C and E. The molecular weights of XPX-2d, XPX-2e, and XP-2 are 133, 195, and 86 kg/mol, respectively. Table 1 summarizes the basic molecular characteristics of these three block copolymers, along with three previously reported samples[19] (XPX-2a, XPX-2b, and XPX-2c), which were further investigated in this study.

Thermal Properties. All XPX and XP materials exhibit similar thermal transitions in DSC as shown in an earlier study[19] (see DSC trace for XPX-2e in the Supporting Information). The melting and crystallization temperatures of the E blocks are around 90 and 55 °C, respectively, and the overall crystallinity of the E blocks is about 20%. The relatively low melting temperature

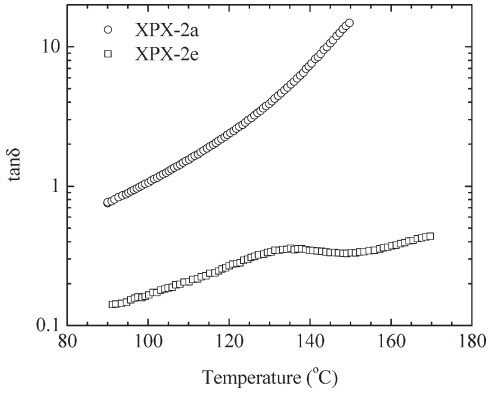

Figure 1. Tan δ for XPX-2a and XPX-2e as a function of temperature determined while cooling at 1 °C/min at a frequency of 1 rad/s.

of poly(ethylene) is due to the random incorporation of ethylethylene repeat units (i.e., addition of 1,2 units in the poly(butadiene) blocks), which interrupts the packing of the poly(ethylene) chains into the crystal lattice thus reducing the crystal size. The mole fraction of 1,2- and 1,4-butadiene addition is about 12% and 88%, respectively, as calculated from ^{1}H NMR. The glass transition of the P blocks occurs at −58 °C. However, the glass transition of the C blocks ($T_g \cong 147$ °C for C homopolymer[45]) was not evident in the DSC traces.

We carried out DMS measurements in order to detect the glass transition of C, which was easily identified in XPX-2d, XPX-2e, and XP-2, but not in the lower M_w samples in the temperature range from 90 to 160 °C. Representative tan $\delta = G''/G'$ traces, obtained while cooling from elevated temperatures at 1 °C/min, are shown in Figure 1 for XPX-2a and XPX-2e, which have the lowest and highest M_w in this series of samples. $T_g \approx 135$ °C for XPX-2e is somewhat lower than that for bulk C homopolymer, which we attribute to the relatively low C M_w along with contact between other saturated polymer blocks. This indicates that the high M_w samples are microphase separated at temperatures higher than T_g of the C block, also consistent with the low M_w samples being in a disordered state.

Rheological Properties. The order−disorder transition usually can be determined using low-frequency DMS measurements based on the transition from nonterminal to liquidlike terminal behavior,[46−48] i.e., storage modulus $G' \sim \omega^2$ and loss modulus $G'' \sim \omega^1$. Isothermal frequency sweep experiments were carried out at several high temperatures. Master curves of G' and G'' are plotted in Figure 2 for XPX-2d and XP-2 as a function of reduced frequency. These master curves were obtained by

dx.doi.org/10.1021/ma2016562 |Macromolecules 2011, 44, 8143–8153

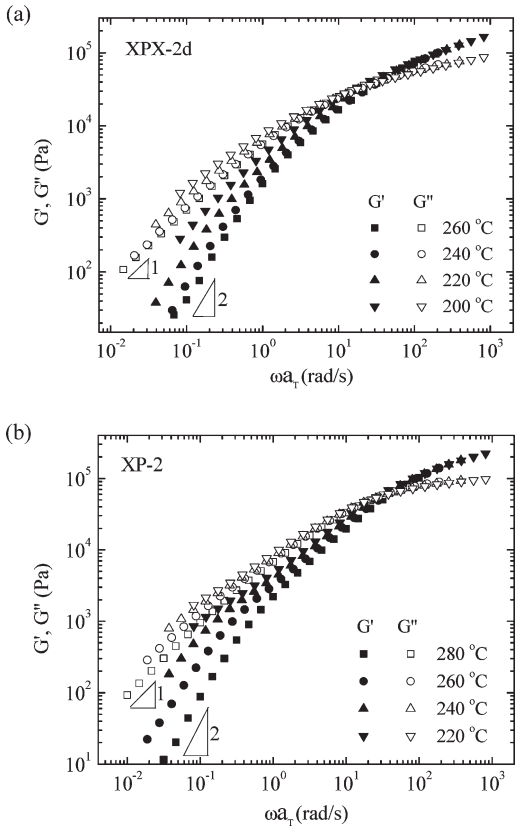

Figure 2. Superposition of G' and G'' against reduced frequency from isothermal frequency sweeps with T_{ref} = 260 °C for XPX-2d (a) and 280 °C for XP-2 (b).

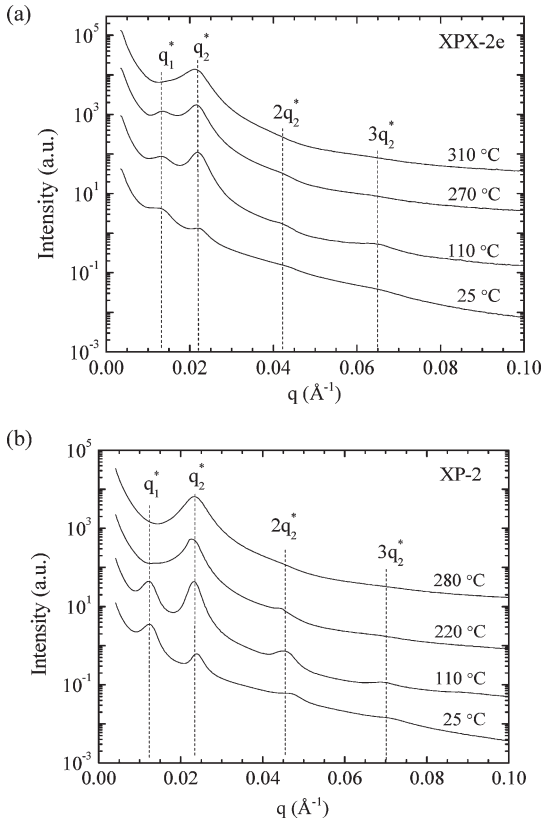

Figure 3. SAXS data for (a) XPX-2e and (b) XP-2 upon heating from room temperature.

superposing the moduli at the highest frequencies using 260 °C (XPX-2d) and 280 °C (XP-2) as the reference temperatures. (Here we note that use of the time−temperature superposition principle with rheologically complex materials is not strictly valid but nevertheless simplifies identification of T_{ODT}.) For XPX-2d, terminal behavior is evident at 260 °C. When the temperature was reduced, the transition from the disordered state to an ordered state could not be established due to an increase in the molecular relaxation time, which shifted the relevant low-frequency regime beyond the lowest attainable limit. Similarly, XPX-2e and XPX-2c produced a liquidlike response at 310 and 220 °C (not shown here), but the transition to an ordered state could not be confirmed at lower temperatures. Nevertheless, on the basis of SAXS experiments (see below), we can narrow the range of possible T_{ODT} values to 270−310 °C for XPX-2e, 220−260 °C for XPX-2d, and 160−220 °C for XPX-2c as listed in Table 1; the two lowest molecular weight materials (XPX-2a, XPX-2b) are melt disordered above 120−140 °C.

For XP-2, liquidlike behavior is evident at 280 and 260 °C (Figure 2b), while an upturn in G' and G'' is (barely) visible at the lowest measured frequencies at 220 °C. The low-frequency response from this material resembles the behavior of diblock copolymers as T_{ODT} is approached in the disordered state,[46] i.e., development of a shoulder in G' at frequencies below the crossover in G' and G'' due to the effects of composition fluctuations, which is also consistent with the SAXS results showing an intermediate state during the order−disorder transition described in the following paragraphs. Although T_{ODT} cannot be established precisely, due to low-frequency limitations, these experiments suggest it lies close to about 200 °C. (Use of the term "order" may not be appropriate for these materials, which are shown below to form microphase-separated structures that lack long-range order.)

Small-Angle X-ray Scattering. Figure 3 shows representative synchrotron SAXS data obtained from XPX-2e and XP-2, first at room temperature and then at progressively higher temperatures. Unlike the SAXS results reported previously for low molecular weight XPX materials, which contain a single peak, these high molecular weight XPX and XP specimens produced SAXS patterns with two principal reflections (q_1^* and q_2^*) at room temperature indicative of two domain periods, d_1 and d_2, where $d_1 = 2\pi/q_1^*$. For XPX-2e and XP-2, the q_2^* peak is clearly associated with two higher-order peaks at $2q_2^*$ and $3q_2^*$, suggesting the formation of a layered morphology. Increasing the temperature to 110 °C, i.e., above the melting temperature of the poly(ethylene) crystals, enhances the scattering intensity of the q_2^* peak relative to the one at q_1^*. We attribute this effect to a decrease in the electron density of the E domains upon melting, which increases the scattering contrast between C and E while reducing the scattering contrast between E and P. These changes provide important clues regarding the underlying morphology as discussed below. At the highest temperatures, 270 °C for XPX-2d (see Supporting Information), 310 °C for XPX-2e, and 280 °C for XP-2, only one broad peak remains at $q = q_2^*$, consistent with a state of disorder as we have seen with the other XPX materials. It is interesting to note that the XP-2 specimen shows both q_1^* and q_2^* peaks and higher order peaks relative to q_2^* at low temperatures, but at 220 °C the q_1^* peak vanishes while peaks at q_2^* and $2q_2^*$ still persist. This suggests an intermediate structure

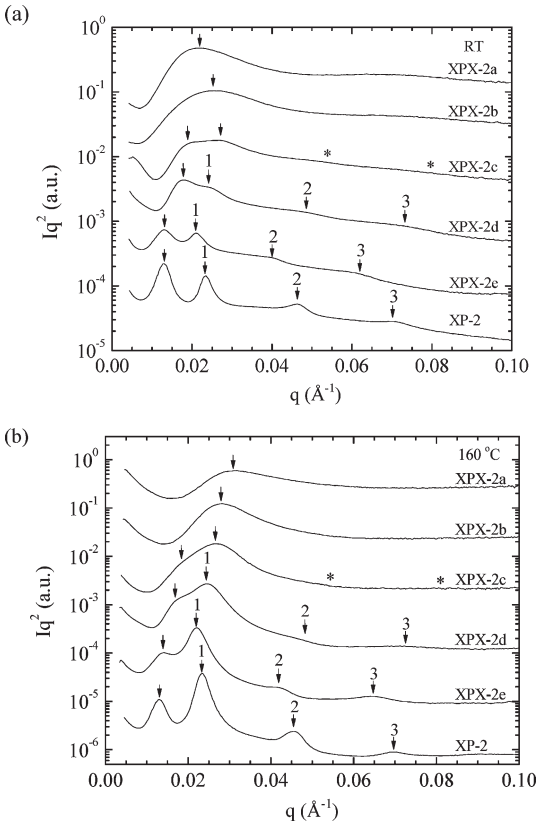

Figure 4. SAXS data for XPX-2 and XP-2 copolymers at (a) room temperature and (b) 160 °C (∗: positions of high-order q_2 peaks based on lamellar structure).

nested between the one with two length scales at low temperatures and the disordered state at 280 °C. We will discuss this in detail later.

The work by Fleury and Bates on CECEC-P and $(CECEC)_2$-P multiblock copolymers with the same overall composition as the materials studied here affords useful comparisons with the present results.[18] The melt disordered undecablock copolymer $(CECEC)_2$-P (M_n = 87 kg/mol) shows one correlation hole peak in the melt, consistent with our results for low-M_n XPX-2 while the melt ordered CECEC-P material with M_n = 120 kg/mol produced SAXS patterns that resemble the four-peak scattering observed for XPX-2e and XP-2 (Figure 3). Fleury attributed the low-q peak (large domain spacing d_1) to correlations between the combined CECEC domains and the P domains and the high-q peaks (small domain spacing d_2) to a layered morphology of C and E within the CECEC portions of the material. By analogy, we believe that for XPX-2e and XP-2 q_1* reflects X−P correlations, i.e., the average distance between the X domains. Similarly, the peak at q_2* can be associated with C−E correlations. This is also consistent with recorded scattering intensity changes related to electron density differences.

Comparisons between SAXS data for all XPX and XP materials at room temperature and 160 °C are illustrated in Figure 4. These results can be divided into two categories: low (XPX-2a, XPX-2b) and high (XPX-2c, XPX-2d, XPX-2e, XP-2) molecular weight compounds. The former exhibit single broad peaks while the latter display two or more reflections. Domain spacings ($d = 2\pi/q^*$) are listed in Table 2 and further analyzed in the Discussion section.

Table 2. Domain Spacings from SAXS Data

sample	d_1 (25 °C) (nm)	d_1 (160 °C) (nm)	d_2 (25 °C) (nm)	d_2 (160 °C) (nm)
XPX-2a			28.9	20.0
XPX-2b			24.4	22.2
XPX-2c	33.6	33.6	23.7	23.5
XPX-2d	37.5	37.5	26.0	25.8
XPX-2e	45.5	45.4	29.0	28.9
XP-2	48.5	48.6	27.2	27.0

Transmission Electron Microscopy. TEM images obtained from XPX-2a, XPX-2d, XPX-2e, and XP-2 are presented in Figure 5. Ideally, the staining process should most darken the P domains followed by the glassy C and semicrystalline E regions.[44] None of the images shown in this illustration contain clearly defined long-range order or easily identified structural features. Fast Fourier transforms (FFT) performed on the TEM images from XPX-2a and XP-2 produced length scales of 23 and 40 nm. XPX-2d and XPX-2e exhibit more diffuse images leading to broader halos and less well-defined length scales by FFT. Within experimental uncertainty these dimensions are consistent with the domain spacings identified by SAXS.[49]

XPX-2a, which has the lowest molecular weight, is melt disordered. Crystallization of the E block during cooling must result in ejection of the adjacent C and P blocks thus inducing microphase separation, consistent with the TEM image from this specimen (panel a). We associate P domains with the dark areas, and X domains with the light portions, which show some color variations, presumably due to segregated E crystals and vitrified C domains. The TEM image of XPX-2d (panel b) also exhibits a disorganized nanoscale structure in this case formed from a microphase-separated melt state due to chemical incompatibility followed by crystallization upon cooling. XPX-2e (panel c) and XP-2 (panel d) show clearly separated X and P domains, where the average spacing between dark and light domains roughly matches the d_1 length scale measured by SAXS (Table 2). In all cases, the morphology is consistent with a bicontinuous arrangement of X and P domains, in agreement with the absence of higher order peaks relative to q_1*. It is difficult to unambiguously differentiate the C and E domains in any of the micrographs. Nevertheless, alternating white and gray stripes can be seen in some regions of the TEM image for XP-2, consistent with the formation of a layered C/E structure as suggested by the SAXS results for XP-2 at room temperature (Figure 3).

Tensile Properties. Figure 6 compares the engineering stress−strain behavior of XPX-2d, XPX-2e, and XP-2 with the three materials described previously (XPX-2a, XPX-2b, and XPX-2c). The results reported here represent averages over at least five specimens tested per material. The tensile properties (listed in Table 3) of all the XPX-2 materials are quite similar, resembling typical thermoplastics, with a Young's modulus (E) between 20 and 30 MPa, yielding (σ_y) at 4−5 MPa, strain hardening beyond about 300% strain, relatively large elongations at break (ε_b = 500−600%), and tensile strengths (σ_{TS}) of 25−35 MPa. (Here we note that these specimens generally fractured at the grip due to tearing or slipping so the apparent fracture strains and ultimate stresses represent minimum values.) In general, the mechanical properties of these five XPX-2 materials, with M_n = 59−195 kg/mol, are essentially indistinguishable, consistent with our assignment of a bicontinuous morphology. However,

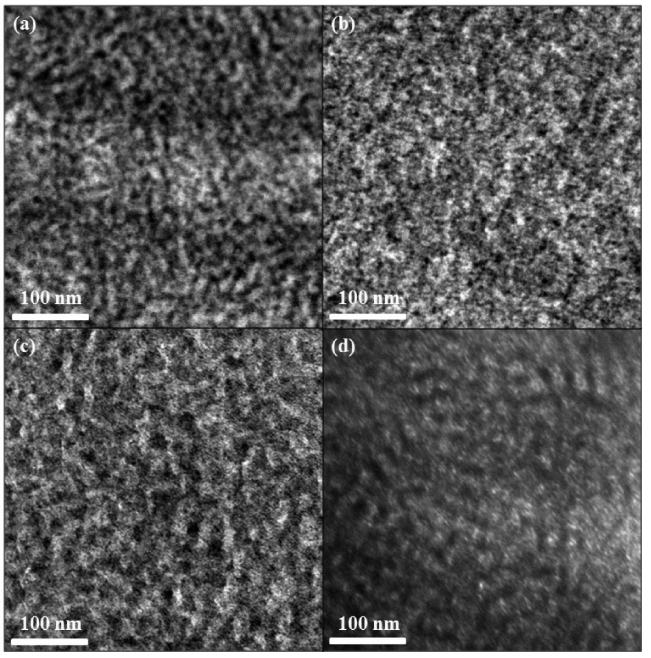

Figure 5. TEM images of XPX-2a (a), XPX-2d (b), XPX-2e (c), and XP-2 (d).

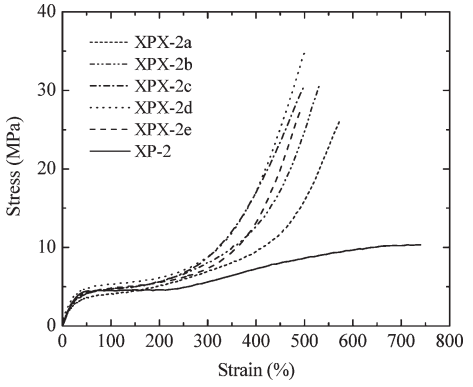

Figure 6. Engineering stress−strain curves of XPX-2 and XP-2 copolymers in tensile tests.

XP-2 shows a decidedly different mechanical behavior notwithstanding a common morphological assignment (see below). The initial stages of deformation up to around 200% strain are quite similar to the XPX-2 materials, but this is followed by strain softening beyond 300% strain and a greater strain at break.

Step-cyclic tests were conducted to probe the recoverability of these materials and selected results are shown in Figure 7. The residual strain (i.e., strain remaining at zero stress) is recorded for each cycle. The initial cycles conducted with small maximum strains are nearly fully recoverable, but as the overall strain increases, plastic deformation leads to nonrecoverable (i.e., residual) strains as illustrated for XPX-2b in Figure 7a; following a 550% strain this specimen recovered all but 180% of the extension upon unloading. We attribute the residual strain to irreversible deformation of the solid E and C domains, opposed by the rubbery recovery of the P blocks. As shown in Figure 7b, the residual strains for XP-2 are much larger than XPX-2b; unloading after 600% strain (and just 9 MPa of stress) results in about 400% residual strain. This implies that the XP-2 is less elastic due to the slippage between P blocks, consistent with the molecular architecture.

Table 3. Mechanical Properties of XPX-2 and XP-2 Materials

sample	E (MPa)	σ_y (MPa)	σ_{TS} (MPa)	ε_b (%)
XPX-2a	19.2 ± 4.5	3.9 ± 0.6	25.8 ± 4.1	616 ± 32
XPX-2b	21.9 ± 1.9	4.5 ± 0.5	30.5 ± 3.1	551 ± 11
XPX-2c	24.0 ± 3.2	4.5 ± 0.9	32.1 ± 5.8	528 ± 19
XPX-2d	33.6 ± 3.9	5.2 ± 1.0	34.0 ± 3.3	505 ± 20
XPX-2e	26.9 ± 6.6	4.6 ± 0.7	26.6 ± 6.9	482 ± 31
XP-2	23.2 ± 2.7	4.3 ± 0.7	10.2 ± 0.5	760 ± 40

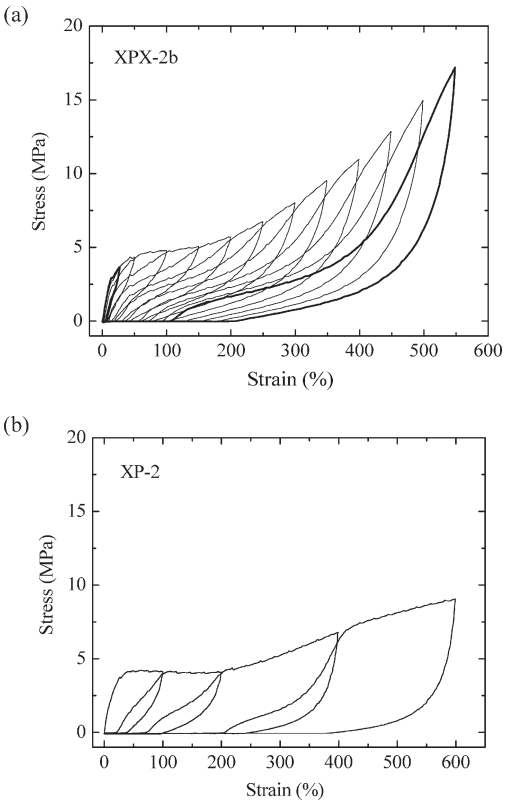

Figure 7. XPX-2b (a) and XP-2 (b) in step-cyclic tests.

Wide-Angle X-ray Scattering (WAXS). The local deformation of XPX-2b as a function of strain was tracked by 2D WAXS, which provides information regarding the structure and development of orientation of poly(ethylene) crystals and to a lesser degree the amorphous domains. Samples were stretched and fixed at specified strains and WAXS data were collected, all at room temperature. Figure 8 shows 2D WAXS patterns obtained from XPX-2b at strains of 0%, 100%, 300%, and 500%. At 0% strain (i.e., before deformation) a diffuse isotropic halo associated with amorphous scattering is evident along with two narrow diffraction rings that can be indexed to the (110) and (200) reflections of orthorhombic poly(ethylene) crystals. Azimuthally integrated WAXS profiles are shown in Figure 9 for the 0 and 500% results. As the specimen is stretched in the horizontal direction, the (110) and (200) reflections intensify and become localized, first at ±60° from the horizontal axis (100% strain) and

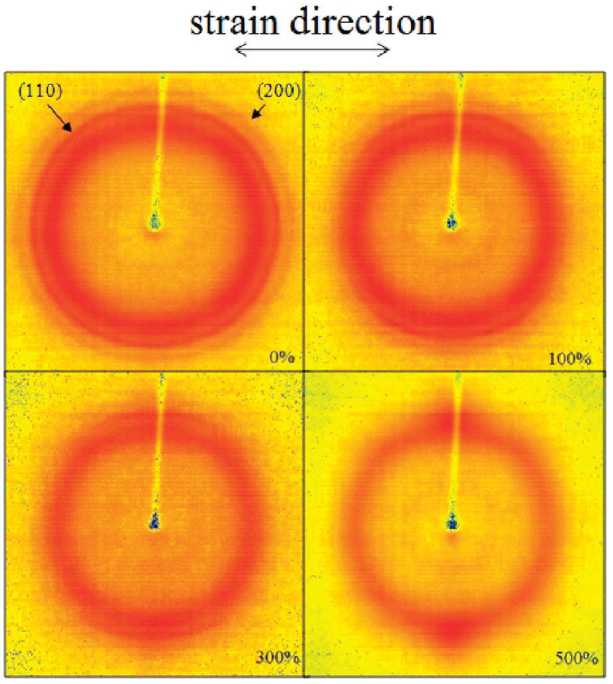

Figure 8. 2D WAXS patterns of XPX-2b at selected strains during uniaxial deformation.

eventually converging on a vertical direction (±90°) at 300% and 500% strains as shown for the (110) scattering in Figure 10. Strong pointlike scattering in the vertical direction at the largest strains is indicative of an orthorhombic-to-monoclinic transformation with crystal stem alignment along the stretching direction.[50−53] This transformation merges the principal monoclinic diffraction peak with the amorphous scattering (see Figure 9). Strain hardening and increased residual strain in XPX-2b coincide with stress induced alignment of the monoclinic E crystals. Significantly, these structural changes in the solid C and E domains occur at about the point where the mechanical response of XP-2 departs from that of the XPX-2 materials (Figure 6). We believe that both strain softening and the larger residual strain in XP-2 reflect a lack of stress transfer across the P domains due to the molecular architecture, i.e., dangling P blocks.

DISCUSSION

Phase Behavior and Morphology. The experimental observations reported here reveal two types of melt state phase behavior for the XPX materials: disordered ($M_n \lesssim 10^2$ g/mol) and ordered ($M_n \gtrsim 10^2$ g/mol). As previously reported (and further substantiated in this study) cooling the low molecular weight materials leads to bicontinuous morphology at room temperature. DSC experiments confirm that crystallization of the E blocks upon cooling triggers microphase separation as confirmed by TEM images. In contrast, the higher molecular weight XPX heptablocks containing equal volume fractions of X and P microphase separate in the melt state ($T > T_g$ and T_m) due to chemical incompatibility. SAXS patterns and TEM images reported here are consistent with the formation of a hierarchical bicontinuous structure devoid of long-range order. Similar experiments with a compositionally symmetric XP tetrablock produced nearly identical results to the high molecular weight

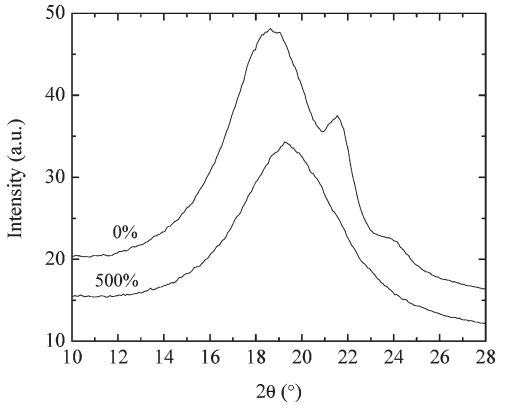

Figure 9. Integrated WAXS profiles of XPX-2b at 0% and 500% strain.

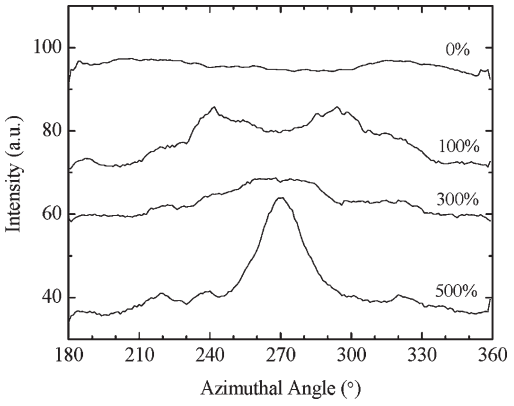

Figure 10. Azimuthal scans of (110) reflection from XPX-2b at selected strains.

XPX materials analogous to the complementary morphological behavior of ABA triblock and AB diblock copolymers.

The temperature dependent binary interaction parameters, χ_{ij}, between C, E, and P have been documented in the literature[54]

$$\chi_{EP} = 8.9T^{-1} - 16.2 \times 10^{-3}$$

$$\chi_{CP} = 15.7T^{-1} - 3.6 \times 10^{-3}$$

$$\chi_{CE} = 29.4T^{-1} - 17.4 \times 10^{-3}$$

based on a 118 Å^3 statistical segment volume. According to these estimates at 280 °C $\chi_{EP} = 0$, $\chi_{CP} = 0.025$, and $\chi_{CE} = 0.036$. At 140 °C the sequence of segment−segment interactions becomes $\chi_{EP} = 0.005$, $\chi_{CP} = 0.034$, and $\chi_{CE} = 0.054$. We have gauged the segregation strength in the XPX polymers based on the parameter χN, where N is the number of statistical segments using two types of block groupings, CEC (end group) and CPC (middle group). For XPX-2e $(\chi N)_{CEC} = 28$ and $(\chi N)_{CPC} = 48$. The random phase approximation (RPA) theory predicts that microphase separation occurs when $\chi N > 18$ for a compositionally symmetric CEC triblock, while for the CPC group (with a C volume fraction of 20%) this condition increases to $\chi N > 40$. Both scenarios anticipate that XPX-2e should be ordered at 310 °C, contrary to the experimental findings. Calculations with XPX-2d and XP-2 lead to similar conclusions.

dx.doi.org/10.1021/ma2016562 |*Macromolecules* 2011, 44, 8143–8153

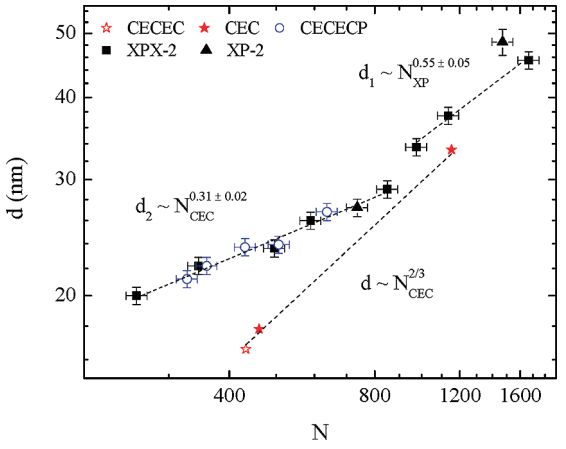

Figure 11. Domain spacings d_1 and d_2 at 160 °C versus degree of polymerization N_{XP} or N_{CEC}, respectively. Previously published periodic spacing d_2 for symmetric CECEC-P materials the lamellar dimension d for symmetric CEC and CECEC are included for comparison.

Obviously this crude approach to estimating the ODT is overly simplistic as it ignores block connectivity and chain stretching. However, a proper self-consistent field theory calculation of the associated phase behavior lies outside the scope of this article. Nevertheless, in a homogeneous melt containing all three block types the C/E interactions will be screened somewhat by more favorable contacts with P segments, qualitatively accounting for the observed phase behavior. Two scenarios are possible upon cooling the disordered melt: microphase separation into two followed by three microdomains or direct transition from disorder to a three-domain configuration.

The SAXS patterns obtained from melt ordered XPX-2e and XP-2 (e.g., T = 110 °C, Figure 3) are nearly identical to those recorded from a melt ordered CECEC-P hexablock copolymer (M_n = 120 kg/mol) by Fleury and Bates.[18] Analogous to that system we believe the current SAXS patterns reflect two scattering correlations: one (q_1^*) associated with the X−P length scale and a second (q_2^*) due to the C−E spacing. Also, the proximity of the single scattering peak from disordered XPX and XP to the melt ordered q_2^* peak confirms that the melt disordered peak stems from correlation hole scattering attributable to the C blocks juxtaposed with E and P. Interestingly, the melt disordered CECEC-P materials showed two correlation hole peaks in the melt (q_1^* and q_2^*) while XPX and XP show only one peak when disordered. Fleury deduced that upon cooling the CECEC portion of the hexablock first segregated from P followed by microphase separation of C and E at lower temperatures, leading to a lamellae-in-lamellae ordered morphology. Thus, despite certain thermodynamic similarities, the architectural variation between CECEC-P and CEC-P (and CECEC-P-CECEC and CEC-P-CEC) seems to generate morphological differences, e.g., hierarchical lamellar order versus a bicontinuous state, respectively.

The melt domain spacings d_1 and d_2 at 160 °C determined by SAXS (Table 2) are plotted versus N_{XP} and N_{CEC}, respectively, in Figure 11, where N_{XP} refers to either the overall degree of polymerization of XP-2 or half the degree of polymerization of the XPX heptablocks and N_{CEC} represents the degree of polymerization of the CEC portion of the XPX compounds. The larger domain spacing scales as $d_1 \sim N_{XP}^{0.55}$, which is intermediate to the RPA predictions for weak ($d \sim N^{1/2}$) and strong ($d \sim N^{2/3}$) segregation. However, the C/E spacings are well represented by $d_2 \sim N_{CEC}^{0.31}$ for both the melt ordered and disordered specimens, a significantly weaker dependence on molecular weight than anticipated by a naive application of the theory. Within experimental uncertainty the d_2 values reported by Fleury and Bates[18] for compositionally symmetric CECEC-P multiblock copolymers (based on half the overall N_{CECEC} values) also exactly conform to this scaling relationship as shown in Figure 11. For comparison, we have added published results for the lamellar spacing of compositionally symmetric CEC and CECEC melts[55,56] to this illustration along with the anticipated (strong segregation limit) scaling $d \sim N^{2/3}$. Clearly, attaching equal volume fraction P blocks to CEC or CECEC dilates the C/E spacing for $N_{CEC} < 1000$; this disparity appears to disappear as N_{CEC} approaches 1000. Also, both XP pseudo-diblock dimensions (d_1 and d_2) are roughly consistent with the XPX data.

Heating XPX-2d, XPX-2e, and XP-2 from 110 °C to elevated temperatures (270−310 °C) results in a single broad SAXS peak (Figure 3) and terminal viscoelastic behavior (Figure 2). We interpret this result as reflecting either weak (simple correlation hole) or strong (composition fluctuations) clustering of the C blocks, characterized by a single correlation length (d_2); note the E and P blocks are chemical isomers with equal electron densities (i.e., no X-ray contrast) and form ideal mixtures (χ_{EP} = 0) at these elevated temperatures. Between high and low temperature limits in the melt state the SAXS data suggest there exists an intermediate state of organization. For simplicity, we focus here on XP-2, but these comments should apply equally to XPX-2d and XPX-2e. The SAXS patterns for XP-2 are distinctly different at 160 and 220 °C, primarily due to the loss of the q_1^* peak at the higher temperature. Yet there is still clear evidence of a week $2q_2^*$ (and possibly a $3q_2^*$) diffraction at 220 °C (and 240 °C). This implies some periodicity in the arrangement of C domains prior to the formation of longer range (d_1) correlations at low temperature. The "fluctuation-like" rheological properties at these temperatures (i.e., low-frequency mode in G' in Figure 2b) also support the notion that there is some additional structural feature present in the melt. We speculate that microphase segregation occurs in two steps as the temperature is lowered: C domains form first and then become correlated in a manner that anticipates the bicontinuous morphology, followed by ejection of the P blocks from the X domains. Self-consistent field theory calculations would be most helpful in clarifying the associated chain conformational changes that accompany these postulated events.

These observations, drawn from the ordered melt state SAXS data along with the TEM evidence obtained from the room temperature specimens, lead us to propose the phase morphology depicted in Figure 12. This illustration portrays composition fluctuations (Figure 12a) at the highest temperatures, then an intermediate state (Figure 12b) with weak correlation between C domains as the temperature is lowered, and finally a bicontinuous structure (Figure 12c) at the lowest temperatures, made up of equal volumes of rubbery P and solid X, with the latter subdivided into periodically spaced glassy C and semicrystalline E domains. We cannot discriminate between sheetlike or tubular domains of X (or P) due to the poorly resolved TEM images. Both could explain the SAXS results found in Figure 3 (q_1^*, q_2^*, $2q_2^*$, $3q_2^*$). However, we favor the conventional symmetric (sheetlike) bicontinuous morphology based on the composition (equal volumes of X and P) and by analogy with the "lamellae-in-lamellae" phase recently documented in CECEC-P heptablock copolymers.[18] Apparently the CEC-P architecture relaxes certain

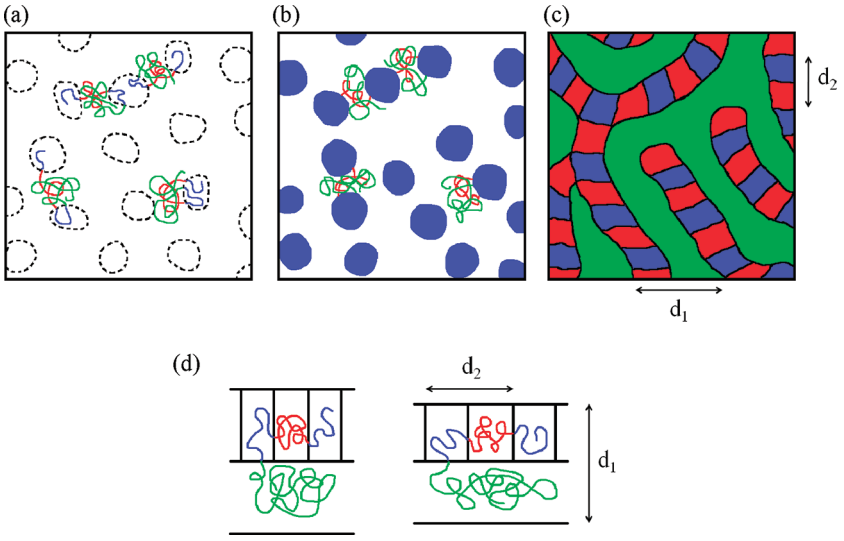

Figure 12. Schematic diagrams of proposed ordering process from (a) composition fluctuation to (b) intermediate state and (c) bicontinuous melt morphology for XP and XPX materials and (d) trade-off between reduced C−E interfacial contact and the spacing d_2. Blue: C; red: E; green: P.

packing constraints that drive three-dimensional order in CE-CEC-P.

We believe the unusual scaling behavior $d_2 \sim N_{CEC}^{0.31}$ results from a tendency to minimize C/E contact and maximize E/P contact as depicted in Figure 12d. Reducing the interfacial area between the C and E domains (i.e., the two most incompatible blocks) leads to an increase in d_2 over the values documented for CEC triblocks and CECEC pentablocks. This simultaneously increases the interfacial area between the blocks with the smallest (E and P) and intermediate (P and C) levels of incompatibility, but at the expense of less favorable chain configurations. Apparently, the net effect of these adjustments on scaling of d_1 is less severe (Figure 11). Interestingly, as the molecular weight increases at constant composition, this effect weakens and d_2 approaches the simpler and better understood CEC and CECEC results. On the basis of the proximity to the fluidlike state at elevated temperatures and consistency of the SAXS results, obtained during heating and cooling, we speculate that the bicontinuous structure depicted in Figure 12c represents an equilibrium melt morphology. Clearly, self-consistent mean-field calculations, and possibly molecular simulations, are required to better understand the trade-offs between interfacial energy and chain stretching that result in this morphology and the observed scaling relationships.

Cooling from the melt state leads to vitrification of C and crystallization of E, which imparts useful mechanical properties. For the melt ordered materials vitrification precedes crystallization, thus preserving the melt morphology as evidenced by the room temperature d_1 and d_2 values. In contrast, cooling the homogeneous specimens (XPX-2a and XPX-2b) results in crystallization of E from a mixed (C, P, and E) phase leading to a departure from the d_2 scaling behavior (see Table 2 or Supporting Information). Nevertheless, crystallization induced microphase separation appears to also produce a bicontinuous, albeit less ordered, structure.[18]

Mechanical Properties. Melt ordered and disordered XPX-2 materials show similar tensile properties (Figure 6) supporting the idea that all these materials share a similar bicontinuous structure, whether induced by chemical incompatibility or crystallization. Hard glassy C domains act as reinforcing fillers physically cross-linking tough E domains in a continuous network embedded in a rubbery P domain. The Young's modulus for the melt ordered XPX specimens, $E = 25 \pm 5$ MPa (Table 3), is comparable to that reported for a polydomain lamellar CPC triblock (E = 28 MPa).[16] Both isotropic morphologies present a statistical distribution of perpendicular and parallel hard domain orientations leading us to expect similar linear elastic moduli. Significantly, the stress−strain response for XP-2 closely tracks the XPX materials up to about 200% strain, consistent with the bicontinuous morphology sketched in Figure 12c. Beyond this point XP-2 strain softens while stretching to 760% elongation before rupture. The analogy drawn earlier regarding morphology in AB and ABA thermoplastics fails to account for these mechanical properties. Lamellar (or bicontinuous) diblocks, such as SI or CP, which combine brittle glassy domain and rubbery domain, are not expected to exhibit resiliency displayed by XP-2. We believe that layering glassy C and semicrystalline E subdomains (including bridging and looping E blocks) impart the same type of mechanical toughness documented in lamellar forming CEC triblock copolymers.[20] Coupling two XP chains together introduces an additional elastic resistance to large deformation through topologically trapped P entanglements, which is evidenced through strain hardening in the XPX-2 copolymers. Both looping and bridging P configurations will contribute to this reinforcing effect, which is entirely absent in the XP material, since all the P blocks are dangling, leading to strain softening.

The influence of these structural features on strain recovery of the XPX-2 multiblock copolymers, along with several other materials (XPX-1, XPX-3, CEC, and CPC, see Table 4 for the molecular characteristics), is shown in Figure 13. All five XPX-2 heptablocks behave similarly during progressive cyclic testing as illustrated in Figure 13 for XPX-2b and XPX-2d. Residual strain develops in two stages (except for CEC) and is correlated with the fraction of semicrystalline blocks (and possibly the overall percentage of solid material, $f_C + f_E$) in the block copolymer. The incremental growth of nonrecoverable deformation at small strains is considerably smaller than above the break point

dx.doi.org/10.1021/ma2016562 |*Macromolecules* 2011, 44, 8143–8153

Table 4. Molecular Characteristics of CPC, XPX-1, XPX-3, and CEC

sample	f_C[a]	f_E[a]	f_P[a]	M_n (kg/mol)[b]	M_w/M_n[b]
CPC	0.30	0	0.70	47	1.03
XPX-1	0.18	0.22	0.60	103	1.11
XPX-3	0.30	0.28	0.42	44	1.21
CEC	0.31	0.69	0	23	1.06

[a] Volume fraction based on ^{1}H NMR of the unsaturated precursors and published densities.[42] [b] Determined by SEC.

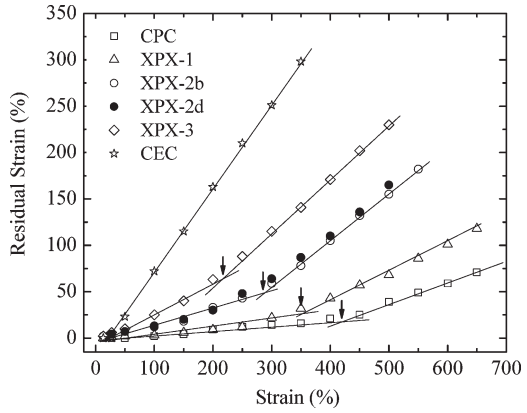

Figure 13. Residual strains versus cycle strain for XPX, CPC, and CEC materials. Two types of deformation are observed while residual strains for CEC increase monotonically.

identified with arrows in Figure 13. On the basis of the WAXS results, we attribute the high strain (hardening) behavior to the severe irreversible disruption of the glassy C domains and distortion and alignment of the E crystals. We associate the strain at the transition (arrows in Figure 13) with the limit of rubber dominated response, which appears to scale with the fraction of P.

In a recent publication, Bishop and Register reported on semicrystalline−glass−rubber−glass−semicrystalline (ABCBA) pentablock copolymers, where microphase segregation is induced by crystallization.[14] Since the hard blocks constitute a minor fraction of the material, the semicrystalline chains become embedded within the glassy blocks forming discontinuous hard domains. This results in TPEs with large strain at break (ca. 500%) and small residual strain (10%), but modest tensile strength (7 MPa) and a rather low modulus (4 MPa). Inclusion of the glassy block mostly eliminates crystal deformation which reduces the permanent set. We believe the advantages of this molecular design are limited to soft TPEs, where the semicrystalline blocks do not contribute to the mechanical properties. XPX and related multiblock copolymers can be tuned across all compositions with continuous control over the physical properties ranging from TPEs to stiff plastics.

CONCLUSION

The structure and mechanical properties of model anionically polymerized and catalytically hydrogenated XPX heptablock and XP tetrablock copolymers (X = CEC) at a constant composition ($f_C \approx f_E \approx 0.25$ and $f_P \approx 0.50$) and varying molecular weight were investigated. Low-M_n samples are melt disordered, while high-M_n samples are melt ordered and produce a doubly periodic structure. Two length scales, $d_1 \sim N^{0.55}$ and $d_2 \sim N^{0.31}$, were identified by SAXS, associated with X−P and C−E domain spacings, respectively. We attribute the unusual d_2 scaling relationship to the combined effects of the sequence of segment−segment interaction parameters, $\chi_{EP} \ll \chi_{CP} < \chi_{CE}$, and the molecular architecture. Minimizing the most unfavorable (C−E) interfacial contacts at constant overall density leads to a bicontinuous morphology with elongated and periodically arranged glassy (C) and semicrystalline (E) domains forming a continuous network embedded in a matrix of rubbery P material. XPX and XP exhibit similar tensile properties up to about 200% consistent with a common morphology as supported by TEM analysis. However, the XP and XPX molecular architectures produce distinctly different stress−strain relationships at larger deformations, attributable to the consequences of dangling versus immobilized P blocks, respectively. Cyclically applied strain recovery experiments show that the residual strain is influenced by the content of solid (C and E) blocks with a transition in behavior before and after strain hardening, which is shown to be associated with the irreversible deformation of E and C domains. These multiblock copolymer materials, prepared from commercially viable commodity monomers, offer highly tunable physical properties along with attractive processing characteristics.

ASSOCIATED CONTENT

Supporting Information. Figures S1−S5. This material is available free of charge via the Internet at http://pubs.acs.org.

AUTHOR INFORMATION

Corresponding Author

*E-mail: bates001@umn.edu.

Present Addresses

[†]The Dow Chemical Company, Freeport, TX 77541.

ACKNOWLEDGMENT

The authors gratefully acknowledge the Medtronic Corporation for financial support of CGA throughout his doctoral research program. F.Z. was supported by the U.S. Department of Energy, Basic Energy Sciences, Division of Materials Science and Engineering, under Contract DEAC05-00OR22725 with UT-Battelle LLC at Oak Ridge National Laboratory. Portions of this work were carried out at the Characterization Facility in the College of Science and Engineering at the University of Minnesota, which receives partial support from the National Science Foundation through the NNIN program and the Materials Research Science and Engineering Center (NSF-MRSEC) at the University of Minnesota (NSF DMR-0212302). SAXS was performed at the DuPont−Northwestern−Dow Collaborative Access Team (DND-CAT) located at Sector 5 of the Advanced Photon Source (APS). DND-CAT is supported by E. I. du Pont de Nemours & Co., The Dow Chemical Company, and Northwestern University. Use of the APS, an Office of Science User Facility operated for the U.S. Department of Energy (DOE) Office of Science by Argonne National Laboratory, was supported by the U.S. DOE under Contract DE-AC02-06CH11357.

REFERENCES

(1) Holden, G.; Legge, N. R.; Quirk, R. P.; Schroeder, H. E. *Thermoplastic Elastomers*, 2nd ed.; Hanser Publishers: New York, 1996.

(2) Scheirs, J.; Priddy, D. B. *Modern Styrenic Polymers: Polystyrenes and Styrenic Copolymers*; John Wiley & Sons: New York, 2003.
(3) Bates, F. S. *Annu. Rev. Phys. Chem.* **1990**, *41*, 525–557.
(4) Bates, F. S. *Science* **1991**, *251*, 898–905.
(5) Matsen, M. W.; Bates, F. S. *Macromolecules* **1996**, *29*, 1091–1098.
(6) Lodge, T. P. *Macromol. Chem. Phys.* **2003**, *204*, 265–273.
(7) Lee, S.; Bluemle, M. J.; Bates, F. S. *Science* **2010**, *33*, 349–353.
(8) Bates, F. S.; Fredrickson, G. H. *Phys. Today* **1999**, *52*, 32–38.
(9) Balsamo, V.; von Gyldenfeldt, F.; Stadler, R. *Macromol. Chem. Phys.* **1996**, *197*, 3317–3341.
(10) Balsamo, V.; von Gyldenfeldt, F.; Stadler, R. *Macromolecules* **1999**, *32*, 1226–1232.
(11) Balsamo, V.; de Navarro, C. U.; Gil, G. *Macromolecules* **2003**, *36*, 4507–4514.
(12) Schmalz, H.; Boker, A.; Lange, R.; Krausch, G.; Abetz, V. *Macromolecules* **2001**, *34*, 8720–8729.
(13) Schmalz, H.; Abetz, V.; Lange, R. *Compos. Sci. Technol.* **2003**, *63*, 1179–1186.
(14) Bishop, J. P.; Register, R. A. *Macromolecules* **2010**, *43*, 4954–4960.
(15) Park, C.; De Rosa, C.; Fetters, L. J.; Thomas, E. L. *Macromolecules* **2000**, *33*, 7931–7938.
(16) Mahanthappa, M. K.; Lim, L. S.; Hillmyer, M. A.; Bates, F. S. *Macromolecules* **2007**, *40*, 1585–1593.
(17) Meuler, A. J.; Fleury, G.; Hillmyer, M. A.; Bates, F. S. *Macromolecules* **2008**, *42*, 5809–5817.
(18) Fleury, G.; Bates, F. S. *Macromolecules* **2009**, *42*, 3598–3610.
(19) Alfonzo, C. G.; Fleury, G.; Chaffin, K. A.; Bates, F. S. *Macromolecules* **2010**, *43*, 5295–5305.
(20) Hermel, T. J.; Hahn, S. F.; Chaffin, K. A.; Gerberich, W. W.; Bates, F. S. *Macromolecules* **2003**, *36*, 2190–2193.
(21) Mori, Y.; Lim, L. S.; Bates, F. S. *Macromolecules* **2003**, *36*, 9879–9888.
(22) Lim, L. S.; Harada, T.; Hillmyer, M. A.; Bates, F. S. *Macromolecules* **2004**, *37*, 5847–5850.
(23) Phatak, A.; Lim, L. S.; Reaves, C. K.; Bates, F. S. *Macromolecules* **2006**, *39*, 6221–6228.
(24) Koo, C. M.; Wu, L. F.; Lim, L. S.; Mahanthappa, M. K.; Hillmyer, M. A.; Bates, F. S. *Macromolecules* **2005**, *38*, 6090–6098.
(25) Koo, C. M.; Hillmyer, M. A.; Bates, F. S. *Macromolecules* **2006**, *39*, 667–677.
(26) Ruokolainen, J.; Makinen, R.; Torkkeli, M.; Mäkelä, T.; Serimaa, R.; ten Brinke, G.; Ikkala, O. *Science* **1998**, *280*, 557–560.
(27) Ruokolainen, J.; ten Brinke, G.; Ikkala, O. *Adv. Mater.* **1999**, *11*, 777–780.
(28) Ikkala, O.; ten Brinke, G. *Science* **2002**, *295*, 2407–2409.
(29) Nap, R, J.; Kok, C.; ten Brinke, G.; Kuchanov, S. I. *Eur. Phys. J. E* **2001**, *4*, 515–519.
(30) Nap, R.; Erukhimovich, I.; ten Brinke, G. *Macromolecules* **2004**, *37*, 4296–4303.
(31) Nagata, Y.; Masuda, J.; Noro, A.; Cho, D.; Takano, A.; Matsushita, Y. *Macromolecules* **2005**, *38*, 10220–10225.
(32) Masuda, J.; Takano, A.; Nagata, Y.; Noro, A.; Matsushita, Y. *Phys. Rev. Lett.* **2006**, *97*, 98301–98304.
(33) Chiang, W.; Lin, C.; Nandan, B.; Yeh, C.; Rahman, M. H.; Chen, W.; Chen, H. *Macromolecules* **2008**, *41*, 8138–8147.
(34) Subbotin, A.; Markov, V.; ten Brinke, G. *J. Phys. Chem. B* **2010**, *114*, 5250–5256.
(35) Wang, L.; Lin, J.; Zhang, L. *Macromolecules* **2010**, *43*, 1602–1609.
(36) Xu, Y.; Li, W.; Qiu, F.; Yang, Y.; Shi, A. *J. Phys. Chem. B* **2010**, *114*, 14875–14883.
(37) Matsuo, M.; Ueno, T.; Horino, H.; Chujyo, S.; Asai, H. *Polymer* **1968**, *9*, 425–436.
(38) Kawai, H.; Hashimoto, T.; Miyoshi, K.; Uno, H.; Fujimura, M. *J. Macromol. Sci., Phys.* **1980**, *B17*, 427–472.
(39) Hotta, A.; Cochran, E.; Ruokolainen, J.; Khanna, V.; Fredrickson, G. H.; Kramer, E. J.; Shin, Y. W.; Shimizu, F.; Cherian, A. E.; Hustad, P. D.; Rose, J. M.; Coates, G. W. *Proc. Natl. Acad. Sci. U. S. A.* **2006**, *103* (42), 15327–15332.
(40) Seguela, R.; Prudhomme, J. *Polymer* **1989**, *30*, 1446–1455.
(41) Mohajer, Y.; Wilkes, G. L.; Wang, I. C.; McGrath, J. E. *Polymer* **1982**, *23*, 1523–1535.
(42) Fetters, L. J.; Lohse, D. J.; Richter, D.; Witten, T. A.; Zirkel, A. *Macromolecules* **1994**, *27*, 4639–4647.
(43) Brandrup, J.; Immergut, E. H. *Polymer Handbook*; John Wiley & Sons: New York, 1989.
(44) Khandpur, A. K.; Macosko, C. W.; Bates, F. S. *J. Polym. Sci., Part B* **1995**, *33*, 247–252.
(45) Zhao, J.; Hahn, S. F.; Hucul, D. A.; Meunier, D. M. *Macromolecules* **2001**, *34*, 1737–1741.
(46) Rosedale, J. H.; Bates, F. S. *Macromolecules* **1990**, *23*, 2329–2338.
(47) Fredrickson, G. H.; Bates, F. S. *Annu. Rev. Mater. Sci.* **1996**, *26*, 501–550.
(48) Kossuth, M. B.; Morse, D. C.; Bates, F. S. *J. Rheol.* **1999**, *43*, 167–196.
(49) Berney, C. V.; Cohen, R. E.; Bates, F. S. *Polymer* **1982**, *23*, 1222–1226.
(50) Kiho, H.; Peterlin, A.; Geil, P. H. *J. Appl. Phys.* **1964**, *35*, 1599–1605.
(51) Wittmann, J. C.; Lotz, B. *Polymer* **1989**, *30*, 27–34.
(52) Shan, H.; White, J. L. *Int. Polym. Process.* **2006**, *4*, 361–373.
(53) Zuo, F.; Burger, C.; Chen, X.; Mao, Y.; Hsiao, B. S.; Chen, H.; Marchand, G. R.; Lai, S.-Y.; Chiu, D. *Macromolecules* **2010**, *43*, 1922–1929.
(54) Cochran, E. W.; Bates, F. S. *Macromolecules* **2002**, *35*, 7368–7374.
(55) Weimann, P. A. PhD Dissertation, University of Minnesota, 1998.
(56) Chu, C. PhD Dissertation, University of Minnesota, 2008.